Surface Science 650 (2016) 210–220

Contents lists available at ScienceDirect

Surface Science

journal homepage: www.elsevier.com/locate/susc

Promotional effects of chemisorbed oxygen and hydroxide in the activation of C–H and O–H bonds over transition metal surfaces

David Hibbitts [a,c], Matthew Neurock [a,b,d,*]

[a] Department of Chemical Engineering, University of Virginia, Charlottesville, VA 22904, United States
[b] Department of Chemistry, University of Virginia, Charlottesville, VA 22904, United States
[c] Department of Chemical Engineering, University of Florida, Gainesville, FL, United States
[d] Department of Chemical Engineering and Materials Science, University of Minnesota, Minneapolis, MN 55455, United States

ARTICLE INFO

Available online 29 January 2016

Keywords:
Density functional theory
Transition metal surfaces
Oxygen
Hydroxide
Charge analysis
C–H and O–H activation

ABSTRACT

Electronegative coadsorbates such as atomic oxygen (O*) and hydroxide (OH*) can act as Brønsted bases when bound to Group 11 as well as particular Group 8–10 metal surfaces and aid in the activation of X–H bonds. First-principle density functional theory calculations were carried out to systematically explore the reactivity of the C–H bonds of methane and surface methyl intermediates as well as the O–H bond of methanol directly and with the assistance of coadsorbed O* and OH* intermediates over Group 11 (Cu, Ag, and Au) and Group 8–10 transition metal (Ru, Rh, Pd, Os, Ir, and Pt) surfaces. C–H as well as O–H bond activation over the metal proceeds via a classic oxidative addition type mechanism involving the insertion of the metal center into the C–H or O–H bond. O* and OH* assist C–H and O–H activation over particular Group 11 and Group 8–10 metal surfaces via a σ-bond metathesis type mechanism involving the oxidative addition of the C–H or O–H bond to the metal along with a reductive deprotonation of the acidic C–H and O–H bond over the M–O* or M–OH* site pair. The O*- and OH*-assisted C–H activation paths are energetically preferred over the direct metal catalyzed C–H scission for all Group 11 metals (Cu, Ag, and Au) with barriers that are 0.4–1.5 eV lower than those for the unassisted routes. The barriers for O*- and OH*-assisted C–H activation of CH_4 on the Group 8–10 transition metals, however, are higher than those over the bare transition metal surfaces by as much as 1.4 eV. The C–H activation of adsorbed methyl species show very similar trends to those for CH_4 despite the differences in structure between the weakly bound methane and the covalently adsorbed methyl intermediates. The activation of the O–H bond of methanol is significantly promoted by O* as well as OH* intermediates over both the Group 11 metals (Cu, Ag, and Au) as well as on all Group 8–10 metals studied (Ru, Rh, Pd, Os, Ir, and Pt). The O*- and OH*-assisted CH_3O–H barriers are 0.6 to 2.0 eV lower than unassisted barriers, with the largest differences occurring on Group 11 metals. The higher degree of O*- and OH*-promotion in activating methanol over that in methane and methyl is due to the stronger interaction between the basic O* and OH* sites and the acidic proton in the O–H bond of methanol versus the non-acidic H in the C–H bond of methane. A detailed analysis of the binding energies and the charges for O* and OH* on different metal surfaces indicates that the marked differences in the properties and reactivity of O* and OH* between the Group 11 and Group 8–10 metals is due to the increased negative charge on the O-atoms (in O* as well as OH*) bound to Group 11 metals. The promotional effects of O* and OH* are consistent with a proton-coupled electron transfer and the cooperative role of the metal-O* or metal-OH* pair in carrying out the oxidative addition and reductive deprotonation of the acidic C–H and O–H bonds. Ultimately, the ability of O* or OH* to act as a Brønsted base depends upon its charge, its binding energy on the metal surface (due to shifts in its position during X–H activation), and the acidity of the H-atom being abstracted.

1. Introduction

Atomic oxygen (O*) is an important intermediate that is formed in many catalytic systems [1] carried out over transition metal catalysts in the presence of oxygen or water including CO oxidation [2–4], methane partial oxidation and reforming [5–10], alcohol oxidation [11–16] or oxygen reduction [16–21]. These reactions are often carried out on supported transition metal nanoparticles which are predominantly comprised of low-index terraces. Madix et al. were the first to show that oxygen bound to Group 11 transition metal (Cu and Ag) surfaces behaves as a Brønsted base and promotes the activation of strong but acidic O–H bonds in water [22,23], methanol [24–26], ethanol [27],

* Corresponding author at: Department of Chemical Engineering and Materials Science, 421 Washington Ave. SE, Minneapolis, MN 55455-0132 United States.
E-mail address: mneurock@umn.edu (M. Neurock).

http://dx.doi.org/10.1016/j.susc.2016.01.012
0039-6028/

formic acid [28–30] and acetic [31] acid, as well as acidic C–H bonds of acetylene [32,33] and propylene [34]. Later work expanded these ideas from the promotional effects of O* on Cu and Ag to Au surfaces involved in the oxidation and coupling of alcohols [15,35–41], oxidation of alkenes [42], and oxidative dehydrogenation of acids [43–47]. Similar results show that O* can also act as a Brønsted base and promote the oxidation of alcohols and the decomposition of organic acids over specific non-noble metal Pd [48–52] and Pt [53] surfaces.

More recent studies, inspired by the work of Madix on Group 11 metals, showed that O* also facilitates activation of O–H bonds of alcohols through a proton-coupled electron transfer like mechanism on Pd and Pt surfaces, and confirmed earlier work on Au close-packed surfaces [15,16]. A key step in forming the active oxygen in the transition state in these reactions involves a shift of O* from its stable three-fold site to a bridge during the activation of C–H bonds of CH_4 over metal-O* site pairs at higher O* coverages on Pt, Rh, and Pd catalysts during the partial oxidation CH_4.

More generally, the reactivity of O* on group 11 and other transition metal surfaces can be extended to other electrophilic adsorbates such adsorbed hydroxide (OH*) and alkoxide (OR*) intermediates that can withdraw electron density from the metal to form negatively charged surface intermediates. Adsorbed hydroxide (OH*) on Group 11 and certain Group 8–10 transition metal surfaces is thought to act as a Brønsted base and promote CO oxidation [54–56], aqueous-phase alcohol oxidation [14–16], electrocatalytic oxidation of alcohols (at elevated potentials or pH) [57–58] as well as electrocatalytic reduction of oxygen [20,59,60]. The surface O* and OH* intermediates in these systems can be formed via the activation of oxygen or water [57,59,60] or introduced by the addition of base (such as NaOH). Similar to O*, the adsorbed OH* withdraws electron density from the surface to form a negatively charged surface intermediate that behaves as a Brønsted base [15,16,57] where it can activate acidic C–H and O–H bonds or carry out nucleophilic attack on CO and CC bonds that form during oxidation or oxidative dehydrogenation reactions [15,61,62]. Similarly, adsorbed alkoxides (OR*) produced in the catalytic conversion of alcohols over Cu supported on silica, have been shown to take on basic character and aid in catalyzing aldol condensation and esterification reactions [63,64].

While previous studies have demonstrated the ability of O*, OH* and, more generally, OR* adsorbates to act as Brønsted bases, these studies have been limited to a relatively few transition metal surfaces. Herein we attempt to understand the influence of the transition metal on the basicity and reactivity of O* and OH* over close-packed Group 8–10 transition metals (Ru, Rh, Pd, Os, Ir, Pt) as well as Group 11 (Cu, Ag, Au) metal surfaces. We carry out first-principle density functional theory (DFT) calculations to systematically compare the barriers to activate the C–H bonds of CH_4 and CH_3* as well as O–H bonds of CH_3OH via metal catalyzed unimolecular decomposition, O*-assisted, and OH*-assisted routes (Eqs. (1)–(3)).

$$R{-}H + {*} \rightarrow R{*} + H{*} \quad (1)$$

$$R{-}H + O{*} \rightarrow R{*} + OH{*} \quad (2)$$

$$R{-}H + OH{*} \rightarrow R{*} + H_2O{*} \quad (3)$$

where $R-H = [CH_3{-}H, {*}CH_2{-}H, CH_3O-H]$

2. Methods

Density functional theory calculations were carried out using periodic, planewave-based methods implemented in VASP [65–68]. The planewaves were constructed with an energy cutoff of 396 eV using projector augmented-wave (PAW) potentials [69,70]. The RPBE form of the generalized gradient approximation (GGA) [71–73] was used to calculate gradient corrections to the exchange and correlation energies as it has been shown to be more accurate than PBE [71] or PW-91 [74] functionals [75]. While RPBE does very well in calculating strongly bound adsorbates, it tends to underpredict the adsorption energy for systems with significant van der Waal interactions. These systems would require the use of hybrid functionals or GGA functionals which specifically account for van der Waals interactions through explicit terms or the introduction of empirical DFT-D corrections. Previous work, however, on O*- and OH*-assisted activations of alcohol molecules on Pd, Pt, and Au reached identical conclusions to the work herein using the PW-91 form of the GGA, [15–16] which 'overbinds' adsorbates [75]. The agreement of this study with those performed previously indicates that the choice of functional does not alter the conclusions of these studies. The closed-packed transition metal surfaces were modeled using a 4×4 unit cell with four atomic metal layers along with a vacuum layer with a size of *3 times* the lattice parameter (at least 10 Å) in between slabs in the z-direction. The bottom two metal layers of the slab were fixed in their bulk positions in order to mimic the bulk surfaces used experimentally. The forces on all of the adsorbate atoms as well as the metal atoms within the top two metal layers were converged to less than 0.05 eV/Å. The wave functions were converged to within 10^{-6} eV and the forces were computed using an FFT grid with a cutoff of twice the planewave cutoff. The first Brillouin zone was sampled using a Monkhorst-pack [74] scheme with a $3 \times 3 \times 1$ k-point mesh. The optimized geometries were subsequently used to carry out single-point calculations with a $6 \times 6 \times 1$ k-point mesh to determine the final electronic energies (E_0). Converged wavefunctions were transformed into a set of localized quasiatomic orbitals (QUAMBOs) [76–79] and used to carry out Löwdin population analyses [80,81] to determine the charges on the individual atoms.

The methyl (CH_3*) binding energies (BE) were calculated with respect to the gas phase CH_3 radical species (BE^{rad}) and also with respect to the more stable gas phase CH_4 and H_2 molecules (BE^{mol}) as shown in Eqs. (1) and (2), respectively.

$$BE^{rad} = E[CH_3{*}] - E[Surf] - E[CH_3] \quad (1)$$

$$BE^{mol} = E[CH_3{*}] - E[Surf] - (E[CH_4] - {}^1/_2 E[H_2]) \quad (2)$$

The binding energies for oxygen were calculated solely with reference to the gas phase free radical O species (BE^{rad}).

A two-stage approach was adopted to locate transition states along the minimum energy reaction paths. The minimum energy reaction path and initial estimates of the transition state were calculated using a nudged elastic band (NEB) [82] calculations with 16 intermediates converged until the force normal to the reaction path was less than 0.3 eV/Å. The NEB transition states were subsequently used as input to the Dimer calculations [83] to isolate and refine the transition state. Dimer calculations were converged until the normal force was less than 0.05 eV/Å with a $3 \times 3 \times 1$ k-point mesh followed by a single-point energy calculation using an $6 \times 6 \times 1$ k-point mesh (similar to the optimizations described above). The mode of the dimer method was examined to ensure that it belonged to the appropriate C–H or O–H bond breaking reactions.

3. Results and discussion

3.1. Electronic nature of O* on Group 8–11 metals

In order to understand the effects of O* and OH* in promoting the surface chemistry, we first examine in detail the changes in the electronic properties and the changes in the binding of these species as we change the metal. More specifically we explore a range of Group 8–10 (Ru, Rh, Pd, Os, Ir, Pt) as well as Group 11 transition metals (Cu, Ag, Au). The results from calculations carried out herein at low coverages indicate that O* preferentially binds to three-fold fcc and hcp sites on the closed-packed (111) fcc or (0001) hcp surfaces (Fig. 1),

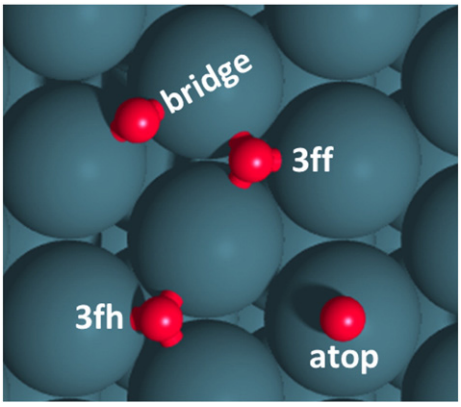

Fig. 1. The binding sites for O* on a closed-packed metal surface. 3ff and 3fh indicate three-fold fcc and three-fold hcp sites, respectively, and differ only in the presence or absence of a metal atom directly beneath the site.

respectively. The binding energy of O* becomes less exothermic in moving from left to right across a row and from 3d to 5d down along a group in the periodic table (Fig. 2A). This was previously attributed to an increase in Pauli repulsion between the electron-rich O* and the d-band of the transition metal, which becomes more filled in moving from left to right in the periodic table [84–87].

O* withdraws 0.5–0.7 e^- from the metal surface on selected Group 8–10 metals (Pt, Pd, Ir, Rh, Os, and Ru) (Table 1). The charge on O* is very similar for Period 4 Group 8–10 metals (−0.56 e^- average) but slightly more negative for Period 5 Group 8–10 metals (−0.63 e^- average). Group 11 metals (Cu, Ag and Au), however, donate significantly more electron density to O* (−1.02 e^- on average) than Group 8–10 metals because of the filled d-band of Group 11 metals (Fig. 2B). The majority of the charge transfer is local, where the three metal atoms bound to the O* are more positively charged with average charges of +1.02, +0.82, and +0.63 for Cu, Ag, and Au (Supporting Info (SI), Table S1). This is consistent with experimental results and the concepts put forth by Madix et al. [1] that the O* creates electron-deficient metal centers that can increase the binding energy of electron-donating molecules (alcohols, nitriles, alkenes) and their activation. The results reported in Fig. 2 show that O* binds more weakly on the Group 11 metals and is more negatively charged, indicating that O* may act as a stronger base on these metals as compared to Group 8–10 metals.

The mobility of O* on a metal surface depends upon the degree to which the binding energy changes as the O* moves from one site to another. The O* diffusion barrier is estimated as difference in energy between O* bound to the stable three-fold fcc or hcp site (reactant state) and O* bound to a neighboring bridge site (transition state). O* is also thought to reside in the bridge sites during O*-assisted C–H and O–H activations [10,15,16]. The energy required for O* to shift from its lowest energy three-fold site to a neighboring bridge site can significantly influence the barriers for O*-assisted C–H and O–H bond activation. Table 1 reports the binding energy of O* at different sites on a 3 × 3 closed-packed surface of various transition metals. The estimated diffusion barriers correlate loosely with the binding energies of O*, with Au(111) having the lowest barrier and Os(0001) having the highest (Fig. S1 in SI). The average charge on the O* ($\bar{z}_{O,8-10}$ on Group 8–10 metals and $\bar{z}_{O,11}$ on Group 11 metals) is slightly lower in the atop site ($\bar{z}_{O,8-10} = -0.50$ and $\bar{z}_{O,11} = -0.89$) compared to the bridge site ($\bar{z}_{O,8-10} = -0.60$ and $\bar{z}_{O,11} = -1.00$) which is very similar to the charge on O* in the three-fold fcc and three-fold hcp sites ($\bar{z}_{O,8-10} = -0.61$ and $\bar{z}_{O,11} = -1.01$) (Table 1, S2 for more details). The relative invariance of the charge of O* between bridge and three-fold sites indicates that the observed site-specificity for O* to act as a Brønsted base in bridging sites is not due to a shift in charge, but instead indicates that an O–M bond must break prior to H-abstraction.

Table 1
Binding energy (BE^{rad}) of O* in atop, bridge, three-fold fcc (3ff) and three-fold hcp (3fh) sites on 4 × 4 closed-packed surfaces. Also shown is the average charge (in e^-) on the O* atoms in each site for the set of Group 8–10 ($\bar{z}_{O,8-10}$) and Group 11 ($\bar{z}_{O,11}$) metals. The most favorable O* BE sites on each metal are shown in bold.

	BE^{rad}				Diffusion barrier[b]
	Atop[a]	Bridge[a]	3fh	3ff	
	eV	eV	eV	eV	eV
Ru(0001)	−4.37	−5.05	**−5.70**	−5.36	0.66
Rh(111)	−3.48	−4.37	−4.73	**−4.85**	0.48
Pd(111)	−2.55	−3.59	−3.92	**−4.08**	0.52
Os(0001)	−4.48	−4.75	**−5.51**	−5.18	0.76
Ir(111)	−3.59	−4.01	−4.35	**−4.54**	0.53
Pt(111)	−2.63	−3.32	−3.56	**−3.91**	0.62
Avg. $\bar{z}_{O,8-10}$	−0.50	−0.60	−0.59	−0.60	
Cu(111)	−2.85	−4.09	−4.38	**−4.46**	0.46
Ag(111)	−1.96	−2.89	−3.10	**−3.17**	0.35
Au(111)	−1.61	−2.27	−2.53	**−2.68**	0.49
Avg. $\bar{z}_{O,11}$	−0.90	−1.00	−1.01	−1.02	

[a] O* was partially constrained in the x,y-plane to sample atop and bridge sites.
[b] Difference in energy between the bridge site and the minimum binding site (3fh or 3ff).

3.2. Chemical nature of OH* on low-index transition metal surfaces

The binding energy of OH* at different sites on various closed-packed metal surfaces is shown in Table 2. The binding energy of OH*

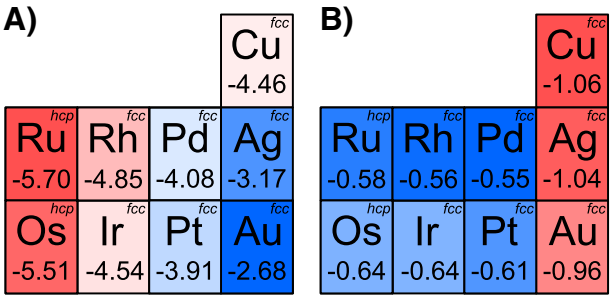

Fig. 2. ***A***) Binding energies (BE^{rad}, eV) and ***B***) charges for O* on 4 × 4 closed-packed Group 9–10 and 11 metal surfaces. The boxes are colored to reflect the O* binding strength as well as the degree of charge transfer. Red refers to the most strongly bound O* intermediates and O* sites with the most basic character whereas the blue refers to the most weakly bound O* intermediates and O* sights with the least basic character.

Table 2
Binding energies (BE^{rad}) for OH* in atop, bridge, three-fold hcp (3fh) and three-fold fcc (3ff) sites on 4 × 4 closed-packed surfaces. The most favorable OH* BE sites on each metal are shown in bold.

	BE^{rad}				
	Atop	Bridge	3fh	3ff	Shift energy[a]
Ru(0001)	−2.58	−2.92	−2.97	**−2.99**	0.41
Rh(111)	−2.27	**−2.49**	−2.33	−2.45	0.22
Pd(111)	−1.86	**−2.03**	−1.81	−1.95	0.17
Os(0001)	−2.61	**−2.70**	−2.58	−2.65	0.09
Ir(111)	**−2.23**	−2.19	−1.74	−1.95	0
Pt(111)	**−1.87**	−1.81	−1.24	−1.54	0
Cu(111)	−1.96	−2.43	−2.55	**−2.59**	0.63
Ag(111)	−1.64	−1.93	−2.00	**−2.03**	0.37
Au(111)	−1.32	**−1.37**	−1.18	−1.24	0.05

[a] Absolute energy difference between atop and minimum binding mode.

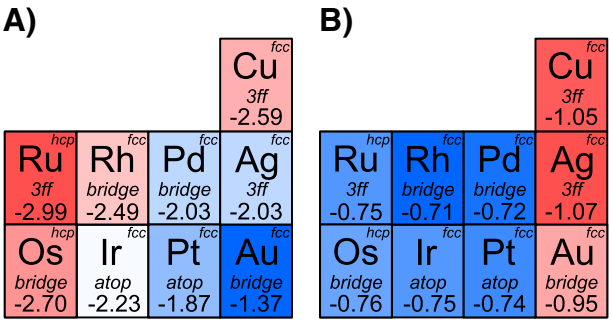

Fig. 3. ***A***) Binding energies (BE^{rad}, eV) and ***B***) charges for OH* on 4 × 4 closed-packed Group 8–10 and 11 metal surfaces. The boxes are colored to reflect the OH* binding strength as well as the degree of charge transfer. Red refers to the most strongly bound OH* intermediates and OH* sites with the most basic character whereas the blue refers to the most weakly bound OH* intermediates and OH* sights with the least basic character.

becomes less exothermic in moving from left to right across a row and from 3d to 5d down a particular column in the periodic table (Fig. 3), as was also observed for O* (Fig. 2). The OH* binding energy correlates directly with the binding energy of O* (Fig. S2 in SI) as can be derived from bond-order conservation (BOC) principles [84–87]. The OH* binding energies are considerably weaker than the O* binding energies and therefore the changes that result in moving from one site to another (atop, bridge, 3-fold) are smaller than those found for O*. As such the diffusion barriers between stable and meta-stable intermediate states are much less than those for O*. The site-preference for OH* shifts toward lower-coordinated bridge and atop positions over three-fold sites in moving from the upper left to the lower right for the block of transition metals in the periodic table. The H-transfer reactions discussed later occur with OH* bound to bridge or atop sites to allow the lone pair of electrons on the O-atom of OH* to interact with the bonds of the reactant adsorbate species. The energy required to shift OH* to its active bridge or atop site is lower (0–0.17 eV) than the energy to shift O* from its stable three-fold site to its active bridge site (0.29–0.75 eV). The increased stability of OH* in bridge or atop sites, compared to the stability of O* in bridge sites, indicates that OH* may be a more reactive co-adsorbate during C–H and O–H reactions.

The O-atom in OH* is negatively charged on Group 8–10 as well as group 11 metals (as was the case for O*) (Fig. 3B). The charge on the O-atom of OH* is more negative (average of −1.02) on Group 11 metals than it is on Group 8–10 metals (average of −0.74) (Fig. 3B) and very similar to the charge on O* on Group 11 metals (Fig. 2B; average of −1.02). On Group 8–10 metals, the charge on the O-atom for OH* is ~0.1 e^- lower (more negative) than the charge on O*. The increased negative charge on the O-atom for OH* over that on O* (over the Group 8–10 metals) is primarily due to the electron transfer from the H-atom to the O-atom in OH* (which donates on average of 0.43 e^- on all of the metals examined, Table S3 in SI).

In summary, O* prefers to sit in highly-coordinated 3fold sites on closed-packed surfaces. For fcc metals, O* prefers three-fold fcc sites and on hcp metals it prefers three-fold hcp sites. Adding H* to the O* (comparing OH* with O*) weakens the interaction of OH* with the metal surface as predicted by bond-order-conservation [84–88]. The weakening has a greater impact upon the high-coordinated binding sites: the binding energy of OH* is, on average, 1.92 eV lower than that for O* in three-fold sites, 1.34 eV lower in bridge sites and 0.79 eV lower in atop sites. This uneven shift results in two important changes: 1) the most stable binding site changes from highly-coordinated three-fold sites for O* to low-coordinated bridge or atop sites for OH* on many metal surfaces; 2) the difference in OH* binding energies at different sites is significantly decreased, resulting in increased mobility of OH* compared to O* on closed-packed metal surfaces. The Löwdin population analysis carried out via QUAMBO shows that Group 11 metals donate more e^- into O* and OH* than Group 8–10 metals. The O-atom in OH* is more negatively charged than O* by ~0.1 e^- for Group 8–10 metals. The H-atom in OH* donates 0.4–0.46 e^- into the O-atom, resulting in a smaller degree of charge transfer from the metal to the OH* as compared to charge transfer from the metal to the O* adsorbate.

3.3. Activation of CH_4 through direct, O*-assisted and OH*-assisted C–H activation

Methane activation over metal surfaces:

$$CH_4 + 2^* \rightarrow CH_3^* + H^* \quad (3)$$

proceeds via an oxidative addition reaction where a surface metal atom inserts into the C–H bond to form the classic three-center (C–M–H) transition state shown in Fig. 4A. We have shown previously that the transition state structures and degree of charge transfer are directly analogous to those reported for organometallic catalysts [89]. Electrons are initially transferred from the CH_4 to the metal as the methane coordinates to the surface. This is followed by significant back-donation of electrons into antibonding σ* states as the C–H bond is elongated. The barriers to activate the initial C–H bond of methane range from 1.05 to 1.14 eV over the Group 8–10 closed-packed metal surfaces, referenced to CH_4 in the gas phase (Fig. 5A). The activation barriers to activate the initial C–H bond of methane over the Group 11 closed-packed metals were calculated to be significantly higher ranging from 1.8 to 2.6 eV due to the filled d-states which result in significant Pauli repulsion, and weaker CH_3* and H* binding to the metal in both the product as well as the transition states. The calculated activation barriers correlate with the reaction energies in a Brønsted Evans Polanyi (BEP) type relationship (Fig. 5A). Similar BEP relationships for methane have also been reported in the literature [87,90–92]. The linear trend, however, is only apparent due to the inclusion of the Group 11 metals; if the Group 8–10 metals are plotted by themselves, the BEP relationship is much weaker. The barriers reported herein are calculated to systematically and reliably compare the energies associated with the three different mechanisms for C–H activation. While the changes in energy from one system to another demonstrate reliable accuracy, the absolute activation energies cannot be directly compared with experiment. Such comparisons would require the explicit treatment of dispersive interactions, entropic effects and zero-point energy corrections as well as the influence reaction environment under working conditions as well as the effects of surface structure. The effects of dispersive interactions, entropic effects, and zero-point energy corrections are expected to be similar for unassisted CH_4 activation, O*-assisted, and OH*-assisted and furthermore are not expected to vary dramatically between activations on these transition metal surfaces. We have carried out such simulations for the activation of methane over supported Pt [7–8] and Pd particles [93] and have shown that these simulations can be used to identify the different kinetic regimes and begin to accurately reflect the apparent activation barrier in each regime.

O*-assisted C–H activation of CH_4 over metal surfaces:

$$CH_4 + * + O^* \rightarrow CH_3^* + OH^* \quad (4)$$

occurs over metal (M) and oxygen (O*) site pairs where the O* shifts from its stable three-fold site to the more active bridge site in order to facilitate C–H activation. The transition state for O*-assisted C–H activation proceeds via the formation of a four-center transition state comprised of M–C, H–M, O–H, and C–H interactions (Fig. 4B on Pd) that is directly analogous to the transition states for σ-bond metathesis in organometallic catalysis [89,94]. The reaction proceeds via a concerted process involving the oxidative addition of the C–H bond of methane to the metal together with a reductive deprotonation over the metal-O* site pair. This is consistent with proton-coupled electron transfer reactions that are well-described by the thermochemical analyses of the free energies for electron and proton transfer [95–96].

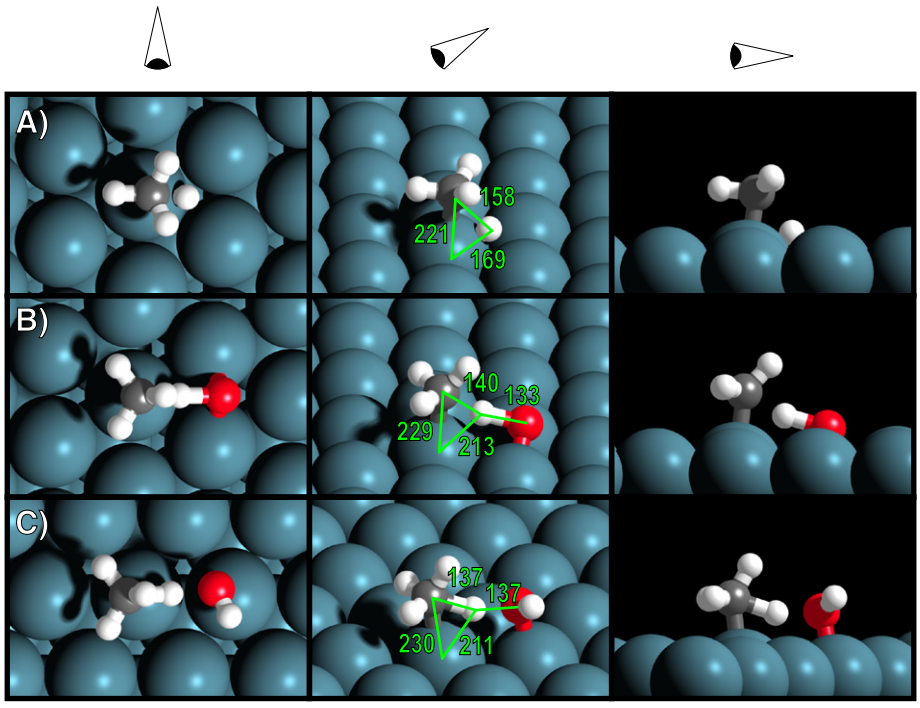

Fig. 4. Transition state structures for the activation of the C–H bond of CH_4 over: ***A)*** metal–metal site pairs (direct), ***B)*** metal-O* site pairs (O*-assisted) and ***C)*** metal-OH* (OH*-assisted) on the Pd(111) surface. Reported bond lengths are given in pm.

O*-assisted CH_4 activation is more endothermic than direct CH_4 activation on Group 8–10 metals and its activation barriers are 0.55–0.88 eV (0.68 eV average) higher (Fig. 5B) than those carried out directly over the metal. The increase in activation barriers is attributed to the non-acidic nature of the C–H bond of CH_4 and the energy penalty (0.48–0.76 eV) associated with shifting the O* from the stable three-fold site to the active bridge site. In contrast, the O*-assisted CH_4 activation on group 11 metals is less endothermic and the activation barriers are lower by 0.27, 1.33 and 0.75 eV for Cu, Ag and Au than those for CH_4 activation carried out directly over the corresponding metal surfaces (Fig. 5B). The energy differences between the barriers for methane activation calculated over the bare metals and those assisted by O* correlate weakly with the binding energy of O* (Fig. 6). The correlation between the activation barriers and the oxygen binding energy is much better if the group 8–10 and group 11 metals are correlated separately. This indicates that factors other than the O* binding energy contribute to the barriers for C–H activation. Cu, for example, is relatively oxophilic and has an O* binding energy that is stronger than that on Pd or Pt. Cu would therefore be predicted to have a lower activation barrier for direct C–H activation than that for O*-assisted C–H activation, similar to the results found on Pd and Pt. The O*-assisted barrier on Cu, however, was actually calculated to be 0.28 eV lower than that for the direct path, in contrast to results on Pd and Pt in which the O*-assisted route has higher barriers than the direct paths (Fig. 6). The charge that forms on O* bound to Group 11 metals (Cu, Ag, and Au (Fig. 2B)) is more negative than the charge that results on the O* bound to Group 8–10 metals. As such, the O* on group 11 metals is much more basic and active in promoting the C–H activation of methane than the O* on group 8–10 metals.

OH*-assisted CH_4 activation:

$$CH_4 + * + OH^* \rightarrow CH_3^* + H_2O^* \quad (5)$$

proceeds over the metal and OH* site pairs. The OH* moves to a near-atop site and leans toward the CH_4 to form the transition state complex

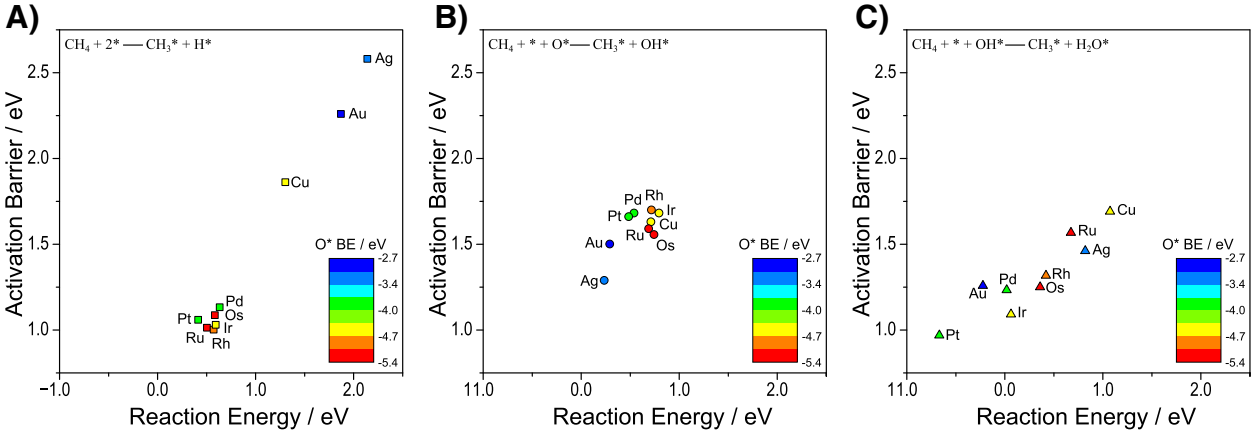

Fig. 5. Activation barriers and reaction energies for the CH_4 activation on Group 8–10 and Group 11 closed-packed metal surfaces. **(*A*)** Direct CH_4 activation (■). **(*B*)** O*-assisted CH_4 activation (●). **(*C*)** OH*-assisted CH_4 activation (▲). Points are colored by the trends in O* binding energy where red refers to the most strongly bound O* and blue refers to the most weakly bound O* (BE^{rad}, eV).

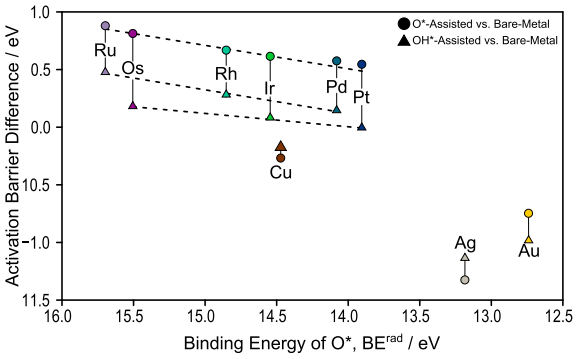

Fig. 6. Difference between O*-assisted and direct CH_4 activation barriers (●) and the difference between OH*-assisted and direct CH_4 activation (▲) compared to the binding energy of O*.

(Fig. 4C for Pd). OH*, like O*, can promote C–H activation by allowing for the concerted oxidative addition and reductive deprotonation of methane over the metal-OH* site pair in a σ-bond metathesis-like mechanism. OH* acts as a Brønsted base and can thus facilitates both C–H and O–H bond activation. Unlike, O*, OH* tends to preferentially bind to the atop and bridge sites where it can act as a Brønsted base. Even in the cases where it binds to the higher fold coordination sites, the barrier for the OH* to shift to an atop site is significantly lower than that for O* to shift with the exceptions of Cu and Ag. As such, OH*-assisted CH_4 activation barriers are lower than O*-assisted barriers for all of the Group 8–10 metals examined and only 0.09 and 0.19 eV higher on Cu and Au, respectively. While the OH*-assisted barriers were lower than the O* barriers, they were still calculated to be higher than those for the direct activation of CH_4 over the Group 8–10 metal surfaces examined (avg: 0.19 eV), with the exception of Pt which has very similar barriers for OH*-assisted and direct CH_4 activation. The OH*-assisted CH_4 activation barriers, on the other hand, were calculated to be significantly lower than both the O*-assisted as well as the direct CH_4 activation barriers on all of the Group 11 metals (with differences of Cu: −0.17 eV, Ag: −1.14 eV, Au: −0.99 eV).

The calculated activation barrier differences between the direct, O*-assisted and OH*-assisted paths depend upon the O* binding energy on each metal and the specific period of the metal, with Period 5 (group 8–10) metals showing a larger difference than Period 6 metals (Fig. 6). This difference between Period 5 and Period 6 metals is due to the relative stability of OH* in the atop position between those two rows. The energy required for OH* to shift from the stable binding mode to an atop site is 0.41, 0.22, and 0.17 eV on Ru, Rh, and Pd (Period 5 Group 8–10 metals). The atop site, however, is much more stable than OH* at other sites on Period 6 metals. OH* preferentially binds to the atop site on Ir and Pt. On Os the preferential bridge site for OH* is only 0.09 eV more favorable than that for the atop site. The penalty for OH* to shift from its most favorable binding site to a vicinal atop site was calculated to be larger on Period 5 metals whereas on Period 6 metals, OH* either prefers atop sites (on Ir and Pt) or can shift to a vicinal atop site with very little energy penalty (as on Os).

3.4. Activation of CH_3 through direct, O*-assisted and OH*-assisted C–H activation*

As was discussed earlier, the direct C–H activation of CH_4 over bare metal surfaces typically proceeds via oxidative addition whereas the O*- and OH*-assisted C–H activation paths proceed via concerted oxidative addition and reductive deprotonation over the metal-O* or metal-OH* site pairs [86]. As O* and OH* are strongly bound to the Group 8–10 transition metal surfaces, they demonstrate only weak Brønsted basicity and do not promote the activation of the non- or weakly acidic C–H bonds such as those in methane. The O* and OH* on the Group 11 metals, however, 1) are much weakly bound to the metal, 2) withdraw considerable electron density from the surface, and 3) show only small enthalpic penalties in shifting from their lowest energy state positions to the more reactive bride and atop sites. As such they demonstrate much greater Brønsted basicity and can promote the activation of non- or weakly acidic C–H bonds such as those in methane.

The average C–M bond length in the transition states involved in the metal atom insertion into the C–H bond of methane averaged over all of the metals studied was calculated to be 2.25 Å. The C–M bond lengths for the transition states involved in the O*- and OH*-assisted activation of methane were calculated to be significantly longer (avg. C–M length of 2.43 Å and 2.40 Å for O*- and OH*-assisted, respectively) as a result of the interactions between the CH_3–H* group and the O* or OH* in the transition state. These longer C–M bonds lead to higher activation barriers as they result in weakly interacting CH_3 groups in the transition state which are less stable and take on more free radical character. Adsorbed alkyls intermediates, on the other hand, are already coordinated to the metal surface via strong covalent C–M bonds (Fig. 7). As such the transition state to activate the C–H bond of a methyl intermediate to form methylidene:

$$CH_3{}^* + {}^* \rightarrow CH_2{}^* + H^* \quad (6)$$

is structurally quite different than the transition state to activate the C–H bond of methane.

The isolated transition state structure for the activation of the C–H bond of CH_3* to form CH_2* (over Pd) which is shown in Fig. 7 is quite different than the transition state to activate the C–H bond of CH_4 shown in Fig. 4A. The C–M bonds as expected are considerably shorter (avg. C–M bonds of 2.09 Å, respectively) and the C–H bond found for the activation of bound CH_3* is considerably longer than the transition state for the activation of CH_3* (average C–H bonds of 1.79 Å across all metals, Fig. 7A shows structure on Pd) compared to the one involved in the activation of CH_4 (average C–H bonds of 1.65 Å across all metals, Fig. 4A shows the transition state structure on Pd). Unassisted CH_3* activation barriers are lower those for CH_4 barriers by an average of 0.67 eV on Group 8 metals (Ru and Os), 0.47 eV on Group 9 metals (Rh and Ir), 0.09 eV on Group 10 metals (Pd and Pt), and 0.23 eV on Group 11 metals (Cu, Ag, and Au). These large differences in activation barriers, favoring the activation of CH_3*, are due to the increased binding energy of the CH_2* species and the stabilization of the CH_2-H* transition state complex on Group 8 and 9, compared to Group 10. The lower barriers to activate the C–H bond of CH_3* verses those for CH_4 are directly related to weaker C–H bond strength for the gas phase CH_3 over that over CH_4. This is consistent with the strong correlation between the activation barriers and the overall reaction energies reported in Fig. 8B.

The C–M bond was calculated to be significantly longer in the transition state for the O*- and OH*-assisted CH_4 activation than it was for direct CH_4 activation. This, however, is not the case for CH_3* activation as the C–M bond is already present in the reactant state. The barriers for the O*- and OH*-assisted activation of CH_3* were much more dependent upon the energy required to shift the O* or OH* to their active sites and their Brønsted basicity at those active sites than the barriers for the O*-assisted activation of methane. The weak O* binding energies on Group 11 metals result in very weak energetic penalties for O* to move to active sites and this leads to the formation of O* sites with greater Brønsted basicity than those for O* on group 8–10 metals. As such, the O*-assisted barriers ($E_{O^*\text{-}assisted}$) are much lower than those for the direct C–H activation of CH_3* (E_{direct}) over the Group 11 metals ($\Delta E = E_{O^*\text{-}assisted} - E_{direct}$ Cu: −0.33 eV, Ag: −1.38 eV, Au: −0.89 eV) (Fig. 9). The differences between the activation barriers for the O*-assisted and direct C–H activation are larger for CH_3* activation than those found for CH_4 activation (Fig. S4, S5 in SI).

O*-assisted CH_3* activation barriers were calculated to be larger than those for the direct CH_3* activation on the Group 8–10 metals. The differences between the O*-assisted and direct routes ($\Delta E = E_{O^*\text{-}assisted}$ −

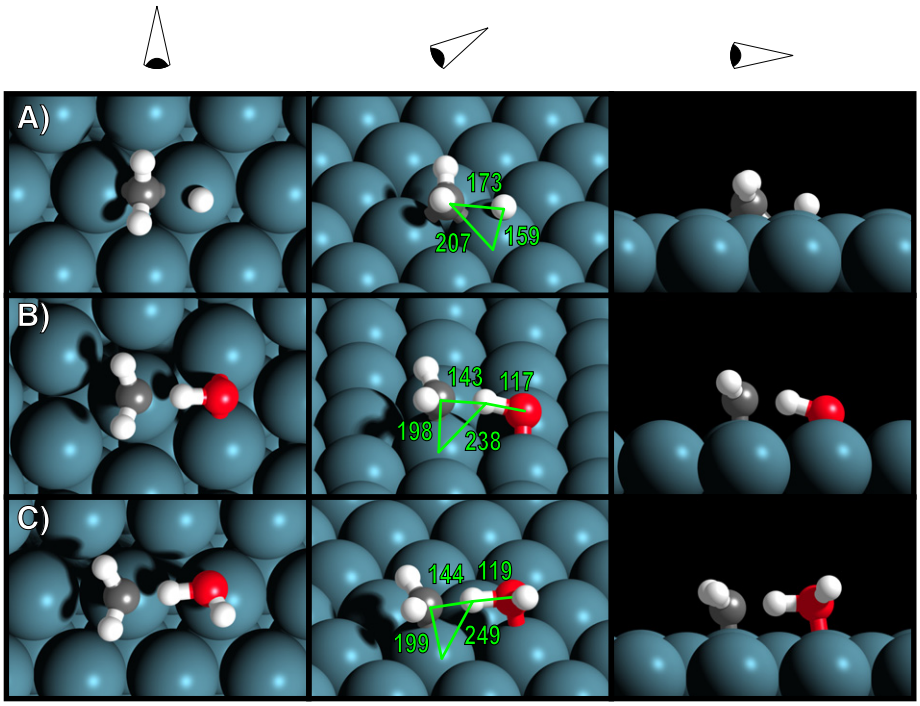

Fig. 7. Transition state geometries for the C–H activation of CH_3* through direct, O*-assisted and OH*-assisted reactions on Pd.

E_{direct}) increase with increasing the O-binding strength (more negative O-binding energies) as is shown in Fig. 9 (the distance between the squares and circles increases as the O* binding energy becomes more negative). Similar results were reported in Fig. 6 for CH_4. The differences between the O*-assisted and direct C–H activation barriers are larger for CH_3* (0.65–1.3 eV in Fig. 9) than for CH_4 activation (0.6–0.9 eV in Fig. 6). OH*-activation shows similar effects to those for O*-activation (see Fig. S4, S5 in SI).

3.5. O–H bond activation of CH_3OH* through direct, O*-assisted and OH*-assisted O–H activation

The activation of acidic O–H bonds such as those of methanol (CH_3OH*) to form methoxide intermediates (CH_3O*) was also examined via the direct, O*-assisted and OH*-assisted paths. Methanol, like other alcohols [15,16,88], adsorbs to metal surfaces via its O-atom sitting in a near-atop position at an angle to the surface. The DFT-calculated binding energies which range from −0.04 to −0.27 eV across the metals examined appear to underestimate the adsorption of methanol and other alcohols due to the absence of van der Waals interactions. Unlike CH_4, where C–H activation occurs over a single metal atom site, direct O–H activation proceeds across 3 metal atoms, where the O of methanol shifts from the atop site to a bridge position, and the H that results ultimately binds to a vicinal three-fold site (Fig. 10). This allows for the methoxy intermediate that forms to reside in its lowest energy state. Direct O–H activation of methanol follows a BEP relationship (Fig. 11B). The calculated barriers on Ir and Pt, however, are slightly lower than their reaction energies would predict, because

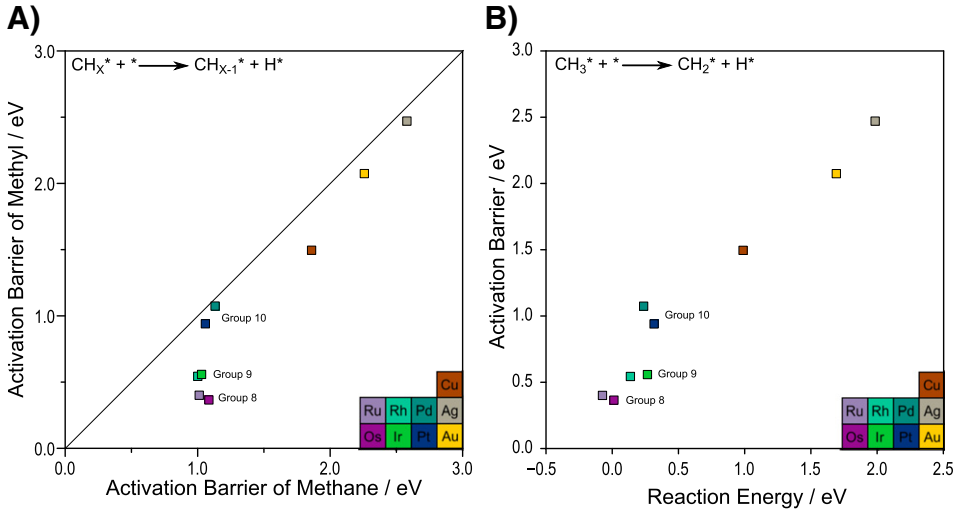

Fig. 8. ***A***) A comparison of the C–H activation barriers of CH_4 and CH_3* on Group 8–10 and 11 metals. ***B***) BEP plot for the C–H activation of CH_3* to form CH_2* (and H*) on Group 8–10 and 11 metals.

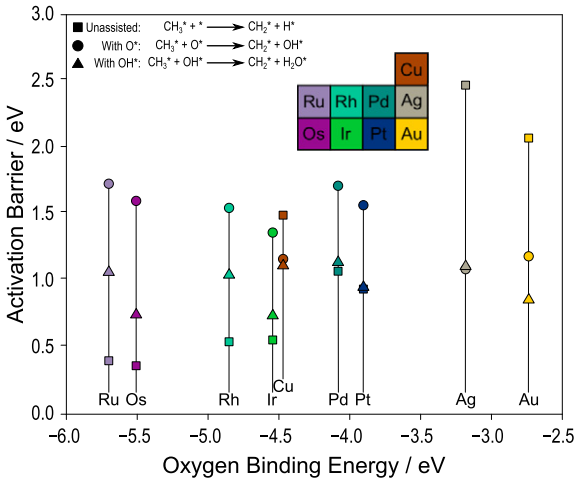

Fig. 9. A comparison of the activation barriers for the C–H activation of CH_3^* through direct, O*-assisted and OH*-assisted reactions on Group 8–10 and Group 11 metals.

the product methoxide (CH_3O^*) that forms is more stable at the atop site on these surfaces (on all other surfaces it prefers to sit three-fold). Cu binds O* stronger than Pt or Pd, despite being a Group 11 metal, and has a reaction energy and activation barrier that is similar to Group 8–10 metals. Comparing the C–H activation of CH_4 with the O–H activation of methanol (Fig. 11A) shows that for most metals, the activation barrier of methanol is lower than that required to activate the C–H bond of CH_4. The gas phase C–H and O–H bond dissociation energies for methane and methanol, respectively are both about the same (~4.55 eV). As such, the lower barriers to activate the O–H of methanol are more likely due to the increased affinity of the metal for the alkoxide over the alkyl intermediate that form. This preference for methanol activation over CH_4 activation is most dramatic for Ag and Cu Group 11 metals, but notably absent from Au; in contrast, Ir, Rh, and Pd show higher O–H activation barriers, indicating these metals have greater affinity for the alkyl intermediate over the alkoxide.

The O–H bond of the alcohol can be activated in the presence of O* by a proton-transfer mechanism where the O* first shifts from its stable three-fold binding site (Fig. 10F for Pd) to a bridging position (Fig. 10G). Once in the bridging position, the terminal proton on methanol transfers from the O–H bond to O* (Fig. 10H), with a transition state that appears as the first maximum shown on the reaction profile (Fig. 10). The second and larger peak involves the breaking of the hydrogen bond that exists between the initial atop-bound methoxide and the bridge-bound hydroxyl intermediates (Fig. 10H) as they diffuse into three-fold fcc positions (Fig. 10J). The diffusion-related barrier associated with breaking the hydrogen bond is not directly related to the basicity of O*, and thus

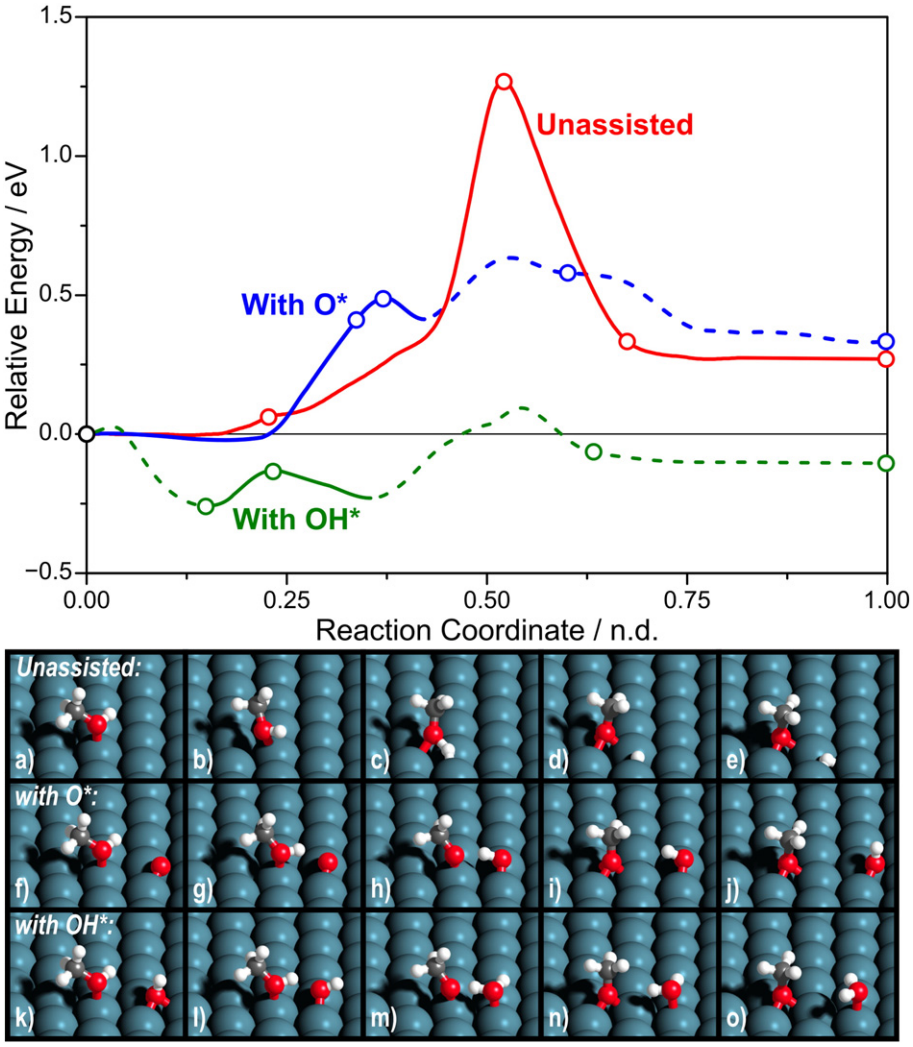

Fig. 10. Reaction pathway for the activation of the O–H bond of methanol, on a clean metal (Pd(111)) surface and through O*- and OH*-abstraction mechanisms. The solid lines of the reaction coordinate section for the O*- and OH*-abstraction mechanisms represent portion of the reaction in which the H-atom is transferred. Dots on the reaction coordinate diagrams indicate that a structure is shown beneath the figure.

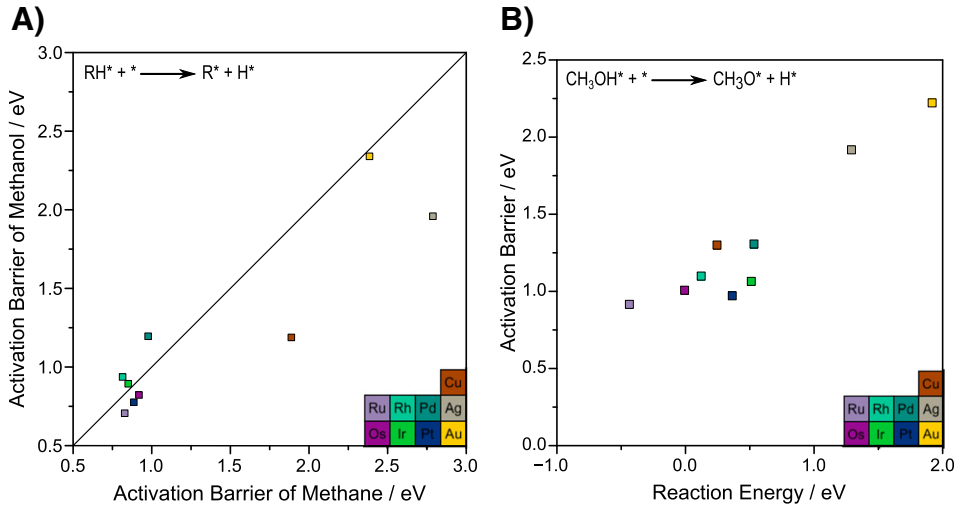

Fig. 11. ***A***) Comparison between unassisted C–H activation of CH_4 and O–H activation of CH_3OH on Group 8–10 and Group 11 metals. ***B***) BEP relationship for the O–H activation of CH_3OH via unassisted O–H activation on Group 8–10 and Group 11 metals.

was not the barrier used in Figs. 11–12. The relative energies of these states vary from metal-to-metal, but the overall mechanism is consistent for the metals examined, with the exception of Ir and Pt where the product CH_3O^* and OH* species prefer to bind atop (rather than in the three-fold sites which the other metals prefer). This change in the adsorption site slightly alters the sequence of the reaction; after the H-transfer step, OH* shifts to the atop position, forming a strong hydrogen bond and CH_3O^* which remains at the atop site.

During OH*-assisted CH_3OH activation, OH* first shifts from its favorable fcc site on Pd to the bridging position adjacent to the alcohol, forming strong hydrogen bonds between the alcohol and OH*. The shift of OH* from the fcc (Fig. 10K) to the bridging position results in the first (very small) barrier (Fig. 10 on Pd). The first minimum in the reaction profile is the state in which the hydrogen bond has been formed which is 0.27 eV more stable than the reactant state on Pd (Fig. 10L). OH* then shifts from the bridge site to an atop position concomitant with a direct proton transfer from the CH_3OH^* to the OH*; this proton transfer and OH* shift is the second maximum (Fig. 10). The resulting CH_3O^* which binds atop of the metal site is hydrogen-bonded to the water that forms at the adjacent metal site (Fig. 10M). The final (and larger) maximum along the reaction coordinate diagram corresponds to energy required to break the hydrogen bond allowing the methoxide to diffuse to the more stable fcc site (Fig. 10N). The

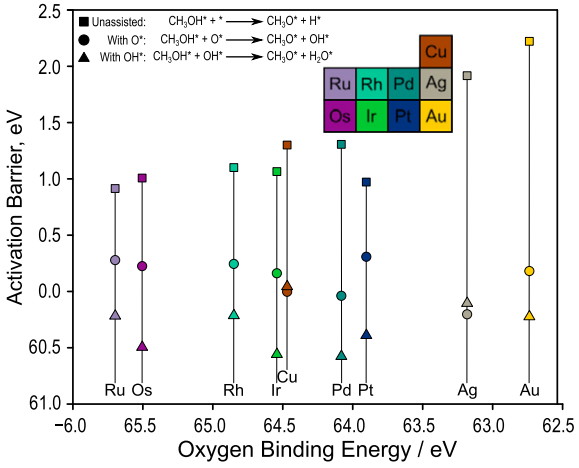

Fig. 12. Activation barrier (referenced to methanol in the gas phase) for the O–H activation of methanol through direct, O*-assisted and OH*-assisted mechanisms for Group 8–10 and Group 11 metals.

reaction sequence on Ir and Pt is slightly different, as it was for O*-assisted activation, due to the fact that both the OH* and CH_3O^* prefer to bind to atop sites on those surfaces. Methanol initially adsorbs at an atop site that is adjacent to the atop OH* and forms a strong hydrogen bond with the OH* which results in methanol binding energies of −0.56 eV and −0.39 eV for Ir and Pt, respectively. There appears to be a near spontaneous proton transfer between bound methanol and OH* in a very weakly activated process with barriers of only 0.03 and 0.02 eV, for Ir and Pt respectively. The resulting methoxide and water that form are very similar in energy to the reactant states. This indicates that on Ir and Pt, this reaction rapidly equilibrates; which would favor the deprotonation of CH_3OH as it has a lower pKa than water.

The results in Fig. 10 show multiple barriers that occur along the reaction paths for the O*- and OH*-assisted CH_3OH activation. Many of these are simply due to the diffusion of species to different binding sites or from changes in H-bonding. We focus here solely on the H-transfer step itself. The H-transfer activation barriers for the direct, O*-assisted and OH*-assisted activation of the O–H bond of methanol (referenced to gas phase methanol) on Pd are 1.20, 0.07 and −0.58 eV, thus indicating that O*- and OH*-assisted paths are much easier than the direct metal catalyzed path for activating methanol. This trend is consistent across the other Group 8–10 metals studied here, with O*- and OH*-assisted CH_3OH activation barriers being 0.72 eV and 1.56 eV lower, respectively, than direct CH_3OH activation (on average). This is in direct contrast to O*- and OH*-assisted CH_4 activations over the group 8–10 metals examined which were all had barriers that were greater than that for the direct path.

The differences between the activation of the O–H bonds in methanol and the C–H bonds of methane are the result of the differences in the acidity of the O–H and C–H bonds that are activated. The O–H hydrogen in methanol is much more acidic (pKa = 17) than the C–H hydrogen of CH_4 (pKa = 56). This is consistent with the results from Madix et al. [1] who showed a direct relationship O* assisted proton transfer for different reactants and their gas phase acid strengths. This is also consistent with the thermochemistry for proton-coupled electron transfer reactions involving C–H and O–H bonds [96–97]. The magnitude of the difference between O*-assisted and direct CH_3OH activation scales with the binding energy of O* (Fig. 12) where the more weakly bound O* results in lower barriers, as was the case for CH_4 activation. The O*-assisted CH_3OH activation barriers ($E_{OH^*\text{-}assisted}$) were calculated to be 0.40, 0.20 and 0.18 lower than those for direct O–H activation (E_{direct}) over the Cu, Ag and Au surfaces respectively. This is analogous to lower barriers reported earlier for the C–H activation barriers for CH_4 over the Group 11 metals. The differences in the barriers for the

O*-assisted and direct O–H activation of CH_3OH, however, are significantly greater in magnitude (with values of $E_{direct} - E_{OH^*\text{-}assisted}$ of 1.25, 2.07 and 1.98 eV for Cu, Ag, and Au, respectively) than they were for C–H activation of methane (with values of $E_{direct} - E_{OH^*\text{-}assisted}$ of 0.27, 1.33 and 0.75 eV for Cu, Ag, and Au). This is consistent with the view that O* acts as a Brønsted base in the activation of both the O–H and C–H bonds, so its effect is directly related to the acidity of the hydrogen that is abstracted. OH*-assisted CH_3OH activation occurs with essentially no barrier once the OH* has diffused to the atop position, regardless of the metal surface. As such, the barriers shown in Fig. 12 represent only the changes in CH_3OH binding energy and the energy required for OH* to diffuse to the atop position. The low barriers indicate that for O–H activation, OH* easily acts as a Brønsted base, abstracting the proton of methanol, on all of the Group 8–10 or Group 11 metals examined.

Conclusions

Electronegative coadsorbates such as atomic oxygen and hydroxyl intermediates that form or are added during the course of reaction can significantly influence the catalytic behavior over different metal surfaces by promoting the activation of acidic X–H bonds. The promotional effects of coadsorbed O* and OH* in activating O–H and C–H bonds are related to their basicity when bound to the metal and are controlled by:

1) The binding energy of O* or OH* on the metal surface. The more weakly bound O* and OH* surface intermediates often participate and aid in the activation O–H and C–H bonds. As such, O* and OH* species which are typically weakly bound to Group 11 metal surfaces show enhanced promotion effects over direct metal activation.
2) The chemical nature of the promoter. OH* which is more coordinatively-saturated than O* is more weakly held to the metal than O* and thus better promotes the activation of O–H and C–H bonds over Group 11 metal surfaces.
3) The energy required to activate the promoter. O* or OH* must shift to the bridging and atop positions, respectively, before they are basic enough to facilitate proton transfer. The energy required to shift O* or OH* to its active site provides a measure of its reactivity. This change in energy is typically proportional to the O* or OH* binding energy.
4) The charge on the O* or OH* bound the metal surface. The O* and OH* are much more negatively charged when bound to Group 11 metals thus increasing their basicity and their ability to promote O–H and C–H activation.
5) The acid strength of the H that is transferred. The more acidic O–H bonds are much more easily promoted by reactions with O* and OH* than weakly acidic C–H bonds.

Alkane activation, which requires the activation and scission of C–H bonds and the transfer of a non-acidic H, preferentially proceeds via the direct metal catalyzed C–H activation as opposed to O*- or OH*-assisted routes over Group 8–10 metals. The basicity of the O* and OH* on the Group 8–10 metals is not strong enough to assisted C–H activation. As such the presence of adsorbed O* or OH* will lower the overall rate of reaction as they will block active surface sites. O*-assisted barriers are significantly lower than direct CH_4 activation barriers on Group 11 metals. This is due to the inert nature of Group 11 metals for C–H bond activation, the weak binding energy of O*, and the high charge transfer to O* on these surfaces. OH* which is more weakly bound and more basic than O* results in lower barriers for C–H activation than O* on all of the metals examined with the exception of Cu and Ag (where it is less mobile and thus less reactive). The subsequent activation of C–H bonds of adsorbed methyl intermediates followed the same trends for direct, O* and OH*-assisted paths as those found for methane activation. The barriers for C–H activation of the methyl for the direct, O*- and OH*-assisted paths, however, were all lower than those for methane. This is due to the shorter M–C distances and the enhanced stabilization of the CH_2* intermediate formed in the transition state for the methyl activation verses the longer M–C bonds and weaker CH_3* interactions for methane activation.

The activation of alcohols proceeds via the activation of the more polar O–H bond. The reaction tends to proceed via a proton transfer where the O*-assisted and OH* assisted O–H activation barriers for CH_3OH are significantly lower than those for the direct O–H activation over the metal for all Group 8–10 and Group 11 metals. The barriers loosely correlate with the binding energy of O*, as the difference in barriers for O*- and direct O–H activations relate to the difference in energy between O* in the three-fold verses the bridge (active) site. OH* which is more mobile and basic than O* on most transition metal surfaces, and thus more active for O–H activation with the exception of Cu and Ag. These trends demonstrate that O* and OH* can act as Brønsted bases on metal surfaces, creating additional routes for the activation of C–H and O–H bonds.

These promotional effects of O* and OH* on catalyst surfaces can lead to 'bimolecular' routes for the activation of C–H and O–H bonds, similar to H*-assisted routes involved in the activation of CO*, NO*, and O_2* on transition metal surfaces [97].

Acknowledgments

We are grateful for the financial support from the National Science Foundation Engineering Research Center for Biorenewable Chemicals (CBiRC) (EEC-0813570) and BP as part of the BP-XC^2 program and computing time from the Environmental Molecular Science Laboratory, a national scientific user facility sponsored by the DOE's (47408) Office of Biological and Environmental Research located at Pacific Northwest National Laboratory. We would also like to thank Dr. Craig Plaisance and Professors Enrique Iglesia and Robert Davis for helpful discussions.

Appendix A. Supplementary data

Supplementary data to this article can be found online at http://dx.doi.org/10.1016/j.susc.2016.01.012.

References

[1] R.J. Madix, J.T. Roberts, in: R.J. Madix (Ed.) Surface Reactions, 34, Springer, Berlin, 1994.
[2] M. Haruta, Catal. Today 861 (1997) 153.
[3] J.M. Schubert, J. Catal. 197 (2001) 113.
[4] T.S. Kim, J.D. Stiehl, C.T. Reeves, R.J. Meyer, C.B. Mullins, J. Am. Chem. Soc. 125 (2003) 2018.
[5] A.B. Mhadeshwar, D.G. Vlachos, Ind. Eng. Chem. Res. 2 (2007) 5310.
[6] M. García-Diéguez, Y.-H. Chin, E. Iglesia, J. Catal. 285 (2012) 260.
[7] Y.-H. Chin, C. Buda, M. Neurock, E. Iglesia, J. Am. Chem. Soc. 133 (2011) 15958.
[8] Y.-H. Chin, C. Buda, M. Neurock, E. Iglesia, J. Catal. 283 (2011) 10.
[9] M.C.J. Bradford, M.A. Vannice, J. Catal. 171 (1998) 69.
[10] C. Buda, D. Hibbitts, M. Neurock, Role of Adsorbed Oxygen During CH_4 Activation Over Transition Metal Surfaces, 2016 (submitted for publication).
[11] M. Besson, P. Gallezot, Catal. Today 57 (2000) 127.
[12] T. Mallat, A. Baiker, Chem. Rev. 104 (2004) 3037.
[13] V.R. Gangwal, J. van der Schaaf, B.F.M. Kuster, J.C. Schouten, J. Catal. 229 (2005) 389.
[14] A. Markusse, B.F.M. Kuster, J.C. Schouten, J. Mol. Catal. A Chem. 158 (2000) 215.
[15] B.N. Zope, D. Hibbitts, M. Neurock, R.J. Davis, Science 330 (2010) 74.
[16] D. Hibbitts, M. Neurock, J. Catal. 299 (2013) 261.
[17] N.M. Markovic, H. Gasteiger, P.N. Ross, J. Electrochem. Soc. 144 (1997) 1591.
[18] M.J. Janik, C.D. Taylor, M. Neurock, J. Electrochem. Soc. 156 (2009) B126.
[19] N.M. Markovic, T.J. Schmidt, B.N. Grgur, H.A. Gasteiger, R.J. Behm, P.N. Ross, J. Phys. Chem. B 103 (1999) 8568.
[20] T. Jacob, Fuel Cells 6 (2006) 159.
[21] J.X. Wang, J. Zhang, R.R. Adzic, Prepr. Pap. — Am. Chem. Soc., Div. Fuel Chem. 49 (2004) 664.
[22] M. Bowker, M.A. Barteau, R.J. Madix, Surf. Sci. 92 (1980) 528.
[23] A. Spitzer, H. Lüth, Surf. Sci. 120 (1982) 376.
[24] I.E. Wachs, R.J. Madix, J. Catal. 53 (1978) 208.
[25] I.E. Wachs, R.J. Madix, Surf. Sci. 76 (1978) 531.
[26] T.E. Felter, W.H. Weinberg, G.Y. Lastushkina, P.A. Zhdau, G.K. Boneskov, J. Hrbek, Appl. Surf. Sci. 16 (1983) 351.
[27] I.E. Wachs, R.J. Madix, Appl. Surf. Sci. 1 (1978) 303.
[28] D.H.S. Ying, R.J. Madix, J. Catal. 61 (1980) 48.
[29] M.A. Barteau, M. Bowker, R.J. Madix, Surf. Sci. 94 (1980) 303.
[30] M. Bowker, R.J. Madix, Surf. Sci. 102 (1981) 542.
[31] M. Bowker, R.J. Madix, Appl. Surf. Sci. 8 (1981) 299.

[32] M.A. Barteau, R.J. Madix, Surf. Sci. 115 (1982) 355.
[33] D.A. Outka, C.M. Friend, S. Jorgensen, R.J. Madix, J. Am. Chem. Soc. 105 (1983) 3468.
[34] M.A. Barteau, R.J. Madix, J. Am. Chem. Soc. 105 (1983) 375.
[35] D.A. Outka, R.J. Madix, Surf. Sci. 179 (1987) 361.
[36] D.A. Outka, R.J. Madix, J. Am. Chem. Soc. 109 (1987) 1708.
[37] R.J. Madix, C.M. Friend, X. Liu, J. Catal. 258 (2008) 410.
[38] B. Xu, L. Zhou, R.J. Madix, C.M. Friend, Angew. Chem. 122 (2010) 404.
[39] B. Xu, X. Liu, J. Haubrich, C.M. Friend, Nat. Chem. 2 (2010) 61.
[40] A. Wittstock, V. Zielasek, J. Biener, C.M. Friend, M. Bäumer, Science 327 (2010) 19.
[41] K.J. Stowers, R.J. Madix, C.M. Friend, J. Catal. 308 (2013) 131.
[42] I.X. Green, M. McEntee, W. Tang, M. Neurock, J.T. Yates Jr., Top. Catal. 56 (2013) 1512.
[43] I.X. Green, W. Tang, M. Neurock, J.T. Yates Jr., Acc. Chem. Res. 47 (2014) 805.
[44] M. McEntee, W. Tang, M. Neurock, J.T. Yates Jr., ACS Catal. 5 (2015) 744.
[45] I.X. Green, W. Tang, M. Neurock, J.T. Yates Jr., J. Am. Chem. Soc. 134 (2012) 13569.
[46] I.X. Green, W. Tang, M. Neurock, J.T. Yates Jr., Faraday Discuss. 162 (2013) 247.
[47] M. McEntee, W. Tang, M. Neurock, J.T. Yates Jr., J. Am. Chem. Soc. 136 (2014) 5116.
[48] N. Aas, M. Bowker, J. Chem. Soc. Faraday Trans. 89 (1993) 1249.
[49] J.L. Davis, M.A. Barteau, Surf. Sci. 256 (1991) 50.
[50] D.H.S. Ying, R.J. Madix, J. Catal. 61 (1980) 48.
[51] S.W. Jorgensen, R.J. Madix, J. Am. Chem. Soc. 110 (1988) 397.
[52] S.W. Jorgensen, R.J. Madix, Surf. Sci. 183 (1987) 27.
[53] N. Kizhakevariam, E. Stuve, J. Vac. Sci. Technol. A 8 (1990) 2557.
[54] M.C. Kung, R.J. Davis, H.H. Kung, J. Phys. Chem. C 111 (2007) 11767.
[55] M. Daté, M. Okumura, S. Tsubota, M. Haruta, Angew. Chem. Int. Ed. Engl. 43 (2004) 2129.
[56] R.A. Ojifinni, N.S. Froemming, J. Gong, M. Pan, T.S. Kim, J.M. White, G. Henkelman, C.B. Mullins, J. Am. Chem. Soc. 130 (2008) 6801.
[57] P. Rodriguez, N. Garcia-Araez, A. Koverga, S. Frank, M.T.M. Koper, Langmuir 26 (2010) 12425.
[58] S.C.S. Lai, S.E.F. Kleijn, F.T.Z. Öztürk, V.C.V.R. Vellinga, J. Koning, P. Rodriguez, M. Koper, Catal. Today 154 (2010) 92.
[59] A. Michaelides, P. Hu, J. Chem. Phys. 114 (2001) 513.
[60] A. Michaelides, P. Hu, J. Am. Chem. Soc. 123 (2001) 4235.
[61] Y. Kwon, K.J.P. Schouten, M.T.M. Koper, ChemCatChem 3 (2011) 1176.
[62] S.C.S. Lai, M.T.M. Koper, Faraday Discuss. 140 (2008) 399.
[63] M.E. Sad, M. Neurock, E. Iglesia, J. Am. Chem. Soc. 133 (2011) 20384.
[64] Z. Tao, D. Hibbitts, M. Neurock, submitted for publication.
[65] G. Kresse, J. Hafner, Phys. Rev. B 47 (1993) 558.
[66] G. Kresse, J. Hafner, Phys. Rev. B 49 (1994) 14251.
[67] G. Kresse, J. Furthmüller, Comput. Mater. Sci. 6 (1996) 15.
[68] G. Kresse, J. Furthmüller, J. Phys. Rev. B 54 (1996) 11169.
[69] P. Blöchl, Phys. Rev. B 50 (1994) 17953.
[70] G. Kresse, D. Joubert, Phys. Rev. B 59 (1999) 11.
[71] J. Perdew, K. Burke, M. Ernzerhof, Phys. Rev. Lett. 77 (1996) 3865.
[72] Y. Zhang, W. Yang, Phys. Rev. Lett. 80 (1998) 890.
[73] B. Hammer, L. Hansen, J.K. Nørskov, Phys. Rev. B 59 (1999) 7413.
[74] H. Monkhorst, J. Pack, Phys. Rev. B 13 (1976) 5188.
[75] K. Yang, J. Zheng, Y. Zhao, D.G. Truhlar, J. Chem. Phys. 132 (2010) 164117.
[76] W.C. Lu, C.Z. Wang, M.W. Schmidt, L. Bytautas, K.M. Ho, K. Ruedenberg, J. Chem. Phys. 120 (2004) 2629.
[77] W.C. Lu, C.Z. Wang, T. Chan, K. Ruedenberg, K. Ho, Phys. Rev. B 70 (2004) 1.
[78] T.-L. Chan, Y. Yao, C. Wang, W. Lu, J. Li, X. Qian, S. Yip, K. Ho, Phys. Rev. B 76 (2007) 205119.
[79] X. Qian, J. Li, L. Qi, C.-Z. Wang, T.-L. Chan, Y.-X. Yao, K.-M. Ho, S. Yip, Phys. Rev. B 78 (2008) 245112.
[80] P.-O. Löwdin, J. Chem. Phys. 18 (1950) 365.
[81] P.-O. Löwdin, Adv. Quantum Chem. 5 (1970) 185.
[82] G. Henkelman, H. Jónsson, J. Chem. Phys. 113 (2000) 9978.
[83] G. Henkelman, H. Jónsson, J. Chem. Phys. 111 (1999) 7010.
[84] C.M. Varma, A.J. Wilson, Phys. Rev. B 22 (1980) 3795.
[85] E.M. Shustorovich, H. Sellers, Surf. Sci. Rep. 31 (1998) 1.
[86] R.A. van Santen, M. Neurock, Molecular Heterogeneous Catalysis: A Mechanistic and Computational Approach, VCH-Wiley, Inc., 2006
[87] R.A. van Santen, M. Neurock, S.G. Shetty, Chem. Rev. 110 (2010) 2005.
[88] E.M. Shustorovich, A.V. Zeigarnik, Russ. J. Phys. Chem. B 1 (2007) 330.
[89] J.F. Hartwig, Organotransition Metal Chemistry, from Bonding to Catalysis, University Science Books, New York, 1994.
[90] B. Xing, X. Pang, G.C. Wang, J. Catal. 282 (2011) 74.
[91] G. Jones, J. Jakobsen, S. Shim, J. Kleis, M.P. Andersson, J. Rossmeisl, F. Abild-Pedersen, T. Bligaard, S. Helveg, B. Hinnemann, J.K. Norskov, J. Catal. 259 (2008) 147.
[92] M. Janik, S. Wasileski, C. Plaisance, M. Neurock, R.A. van Santen, submitted for publication.
[93] Y.H. Chin, C. Buda, M. Neurock, E. Iglesia, J. Am. Chem. Soc. 135 (2013) 15425.
[94] R. Waterman, Organometallics 32 (2013) 7249.
[95] J. Mayer, Acc. Chem. Res. 44 (2011) 34.
[96] J. Mayer, Annu. Rev. Phys. Chem. 55 (2004) 363.
[97] D. Hibbitts, E. Iglesia, Acc. Chem. Res. 48 (2015) 1254.